

Theory of Membraneless Electrochemical Cells

William A. Braff^a, Cullen R. Buie^a, and Martin Z. Bazant^{b,c,z}

Departments of ^aMechanical Engineering, ^bChemical Engineering and ^cMathematics,

Massachusetts Institute of Technology, Cambridge, MA 02139, USA

^zemail: bazant@mit.edu, phone: 617-258-7039

Abstract

A mathematical theory is presented for the charging and discharging behavior of membraneless electrochemical cells, such as flow batteries and electrolyzers, that rely on slow diffusion in laminar flow to separate the half reactions. Ion transport is described by the Nernst-Planck equations for a flowing quasi-neutral electrolyte with heterogeneous Butler-Volmer kinetics. Analytical approximations for the current-voltage relation and the concentration and potential profiles are derived by boundary layer analysis (in the relevant limit of large Peclet numbers) and validated against finite-element numerical solutions. Both Poiseuille and plug flows are considered to describe channels of various geometries, with and without porous flow channels. The tradeoff between power density and reactant crossover and utilization is predicted analytically. The theory is applied to the membrane-less Hydrogen Bromine Laminar Flow Battery and found to accurately predict the experimental and simulated current-voltage data for different flow rates and reactant concentrations, during both charging and discharging. This establishes the utility of the theory to understand and optimize the performance of membrane-less electrochemical flow cells, which could also be extended to other fluidic architectures.

Introduction

Since they were first developed over ten years ago, membrane-less laminar-flow electrochemical cells have attracted considerable attention.¹⁻⁵ Compared to traditional electrochemical cells, these systems eliminate the need for a membrane by relying on laminar flow and the slow molecular diffusion of reactants to ensure separation of the two half-reactions. Apart from the cost reductions that go along with removing the most expensive component of an electrochemical stack,⁶ balance of plant is simplified by avoiding any membrane hydration requirements. Chemical limitations imposed by the membrane are also eliminated, allowing for the use of a wide range of electrolytes, fuels, oxidants, and catalysts.⁷⁻¹²

The inherent advantages of this technology for micro and small-scale mobile power applications were identified early in the development of these systems,¹ but the mass transfer limitations present in these devices have limited their overall power density and applicability. A number of new concepts have been incorporated to improve performance, including porous separators to minimize crossover,^{11,13} air-cathodes to enhance oxygen transport,¹⁴ patterned electrodes to enhance chaotic mixing,^{15,16} and flow-through porous electrodes to enhance fuel utilization,^{1-5,17,18} but the fundamental limitations of the technology largely remain. Previous efforts to model laminar flow systems have focused on either channel geometry and flow optimization,^{6,19-21} or more detailed examination of the impact of reactant crossover and diffuse charge.^{7-12,22,23} However, these models have required computationally intensive numerical techniques, with solutions requiring as much as several hours of processor time to compute, and they provide limited analytical insights.

The purpose of this work is to derive accurate scaling laws and theoretical guidelines that can be applied to the future design of membraneless electrochemical cells. The ability of these systems to maintain reactant separation is of particular importance, and previous work has independently established scaling laws for mixing colaminar flow in microchannels.^{1,24,25} We present numerical and approximate analytical solutions of a general mathematical model that couples these scaling laws to a Nernst-Planck description of ion transport. The theory is developed for laminar electrochemical cells with Poiseuille or plug flow between flat electrodes, but the model equations could be applied to any fluidic architecture with appropriate flow profiles.

The general theory is illustrated by successful application to the Hydrogen Bromine Laminar Flow Battery (HBLFB).^{11,13,24,25} The HBLFB uses a membrane-less laminar flow design with concentrated liquid bromine serving as the oxidant and gaseous hydrogen as the fuel. The system is reversible, producing hydrobromic acid in discharge mode and recovering bromine and hydrogen in charging mode, with high round-trip efficiency. Although this system differs from many existing membraneless electrochemical cells in that it uses a liquid oxidant and gaseous fuel, the rapid reaction kinetics at both electrodes minimizes activation losses and make for an appealing model system. These characteristics have also been shown to allow the HBLFB to achieve power densities as high as 794 mW/cm^2 , with a round-trip voltage efficiency of 90% at 25% of peak power in its first iteration.^{14,26} The full model in two dimensions can be solved numerically using finite elements to predict the performance of the HBLFB, as well as to better understand the sources of loss and how they can be mitigated. The focus of this work, however, is to derive simple, but accurate, approximate solutions by boundary-layer analysis, which can be used to quickly establish the relative importance of the various sources of loss and interpret experimental data. Although there has been

some work analyzing the current-voltage behavior of laminar flow electrochemical cells, this appears to be first study to provide closed-form analytical solutions.^{15,16,27} By accurately predicting the behavior of the HBLFB with minimal computational expense, the analytical model can serve as a guide for future design of laminar flow electrochemical cells.

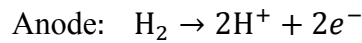
Mathematical Model

The laminar flow electrochemical cell consists of two flat electrodes with flowing electrolyte separating them. The flow within the channel is assumed to be fully developed and laminar. The length of the channel L is assumed to be much greater than the spacing h between the electrodes or the channel width w , so that edge effects can be neglected. Two canonical cases of unidirectional flow are considered. In the first case, $h \ll w$, so the flow is roughly uniform in the z direction, and adopts a parabolic velocity profile between the electrodes as shown in Figure 1a. In the second case $w \ll h$, and the velocity profile can be depth-averaged in the z direction to arrive at a uniform velocity profile between the electrodes as shown in Figure 1b. This Hele-Shaw type flow can generally be described as a potential flow. There is a third case, in which a channel of arbitrary shape contains a porous medium, and the flow obeys Darcy's Law. The flow can be treated in the same manner as the potential flow case, as shown in Figure 1c. Ion transport is governed by the Nernst-Planck equations, which predict concentration polarization, leading to variations in bulk conductivity.²⁸ The electrostatic potential is determined by bulk electroneutrality across the entire channel, since the typical channel dimensions (~ 100 micron – 1 cm) are much larger than the Debye screening length (~ 1 nm). Frumkin effects of double-layer charge on reaction kinetics are also neglected.^{29,30} These approximations become more accurate at high salt concentrations, but dilute

solution theory is applied for simplicity here. It would be straightforward to account for activity coefficient corrections on transport²⁸ and reaction kinetics³¹ in numerical simulations, but analytical progress would be more difficult.

Example: Hydrogen Bromine Laminar Flow Battery

For the HBLFB during discharge, the two half-cell reactions are the oxidation of hydrogen at the anode, and the reduction of bromine at the cathode.



For the purpose of this work, the electrodes are assumed to be thin so the reactions can be treated as heterogeneous. A microporous anode is assumed to provide sufficient hydrophobicity such that it creates a thin interface between liquid electrolyte in the open channel and gaseous hydrogen in the electrode. Therefore, no gas intrudes into the channel, and no liquid intrudes into the electrode. The entire cell is assumed to be isothermal and isobaric at standard temperature and pressure. The electrolyte is assumed to be quasineutral at high salt concentration, and reaction kinetics are typically fast compared to bulk diffusion.³² Reaction rate constants are estimated based on values quoted in the literature, although because activation losses are minimal in this system, the model is not sensitive to these values.³³ The relevant parameters and their nominal values are listed in Table 1.

Governing Equations in the Electrolyte

The species present in the channel are the reactant bromine and the product hydrobromic acid. The geometry of the channel is shown schematically in Figure 1a, so

fluid flow is assumed to be fully developed Poiseuille flow in a channel, and is treated as a model input.

$$\vec{u} = 6U(y/h - y^2/h^2)\hat{i} \quad [2]$$

Reactions occur only at the boundaries, so species and current conservation is maintained within the channel. Species flux \vec{N}_i and ionic current \vec{J} can be expressed by applying dilute solution theory and using the Nernst Planck equations in terms of the parameters listed in Table 1, species concentrations c_i , and dimensionless ionic potential $\tilde{\phi}$, scaled to the thermal voltage RT/F .

$$\begin{aligned} \vec{N}_{H+} &= -D_{H+}(\nabla c_{H+} + c_{H+}\nabla\tilde{\phi}) + \vec{u}c_{H+} \\ \vec{N}_{Br-} &= -D_{Br-}(\nabla c_{Br-} - c_{Br-}\nabla\tilde{\phi}) + \vec{u}c_{Br-} \\ \vec{N}_{Br2} &= -D_{Br2}\nabla c_{Br2} + \vec{u}c_{H+} \\ \vec{J} &= F(\vec{N}_{H+} - \vec{N}_{Br-}) \end{aligned} \quad [3]$$

Because electroneutrality and a binary electrolyte are assumed, the concentration of protons and bromide ions are equal, and the governing equations can be simplified by defining an ambipolar diffusion coefficient $D_{HBr} = 2D_{H+}D_{Br-}/(D_{H+} + D_{Br-})$.³⁴

$$\begin{aligned} \vec{N}_{HBr} &= -D_{HBr}\nabla c_{HBr} + \vec{u}c_{HBr} \\ \vec{N}_{Br2} &= -D_{Br2}\nabla c_{Br2} + \vec{u}c_{Br2} \\ \vec{J} &= F(D_{H+} - D_{Br-})\nabla c_{HBr} + F(D_{H+} + D_{Br-})c_{HBr}\nabla\tilde{\phi} \end{aligned} \quad [4]$$

Anode Boundary Conditions

The anode itself is not explicitly included in the model, but the potential drop across the interface between the grounded anode and the electrolyte determines the ionic potential ϕ at the boundary $y = h$. The potential drop is a function of the equilibrium half-cell potential $\Delta\phi_a^{eq}$, modeled by the Nernst equation, and activation overpotential η_a ,

modeled by the symmetric Butler-Volmer equation. These quantities are coupled to both the local acid concentration c_{HBr} and the local current density $j = \hat{n} \cdot \vec{j}$ normal to the boundary.

$$\begin{aligned}\varphi(x, y = h) &= -\varphi_a^{eq}(c_{\text{HBr}}) + \eta_a(c_{\text{HBr}}, j) \\ \varphi_a^{eq}(c_{\text{HBr}}) &= \varphi_a^0 + \frac{RT}{F} \ln(c_{\text{HBr}}) \\ \eta_a(c_{\text{HBr}}, j) &= \frac{RT}{F} \sinh^{-1} \left(\frac{j}{2K_a^0 c_{\text{HBr}}} \right)\end{aligned}\quad [5]$$

These three equations can be combined to form a coupled, nonlinear boundary condition for potential at $y = h$, and simplified by noting that standard potential at the anode is zero volts referenced to the standard hydrogen electrode.

$$j = 2K_a^0 c_{\text{HBr}} \sinh \left(\frac{F\varphi}{RT} + \ln c_{\text{HBr}} \right) \quad [6]$$

Faraday's Law determines species conservation by noting that at the anode, the active species is protons, while the bromide ions are static, and, assuming there is no crossover, bromine plays no role in the reaction.

$$\begin{aligned}N_{\text{Br}_2} &= 0 \\ N_{\text{Br}^-} &= 0 \\ N_{\text{H}^+} &= j/F\end{aligned}\quad [7]$$

These equations for bromide and proton flux can be combined using the ambipolar diffusion coefficient.

$$N_{\text{HBr}} = -\frac{D_{\text{HBr}}}{2D_{\text{H}^+}} \frac{j}{F} \quad [8]$$

Cathode Boundary Conditions

The cathode adds in the consumption of bromine, but is otherwise very similar to the anode. The potential boundary condition at $y = 0$ reflects the concentration dependent

and spatially varying equilibrium potential of the bromine reduction reaction, φ_c^{eq} , and the non-zero cathode potential, φ_{cell} , which is a model input parameter.

$$\varphi(x, y = 0) = \varphi_{cell} - \varphi_c^{eq}(c_{Br_2}, c_{HBr}) - \eta_c(c_{Br_2}, c_{HBr}, j) \quad [9]$$

This expression can be rewritten as a coupled, nonlinear, mixed boundary condition by combining the impact of bromine activity with the equilibrium potential and activation overpotential.

$$j = -2K_c^0 \sqrt{c_{Br_2} c_{HBr}} \sinh\left(\frac{F}{RT}(\varphi + \varphi_c^0 - \varphi_{cell}) + \frac{1}{2} \ln\left(\frac{c_{Br_2}}{c_{HBr}^2}\right)\right) \quad [10]$$

Faraday's Law again describes species conservation, and the species flux can be expressed as an effective ambipolar flux by observing that the active species at the cathode is the bromide ion, with no contribution from protons. An interesting aspect of this result is that although the ionic flux at the cathode and anode are identical for a given current, the apparent ambipolar flux at the cathode is larger due to the slower diffusion of bromide ions relative to protons.

$$\begin{aligned} N_{Br_2} &= \frac{j}{2F} \\ N_{HBr} &= -\frac{D_{HBr}}{2D_{Br^-}} \frac{j}{F} \end{aligned} \quad [11]$$

The standard potential of aqueous bromine is known to be 1.087 V.³⁵ However, in the presence of bromide ions, bromine complexes into tribromide with an equilibrium coefficient of 17 L/mol.³⁶ At the concentrations probed in this study, tribromide replaces bromine as the dominant reactant species in the oxidant stream. Past efforts with numerical simulations have attempted to model how homogeneous reactions between bromine and tribromide affect the behavior of bromine reduction. However, these simulations are only tractable under very limited circumstances and are completely dependent on the uncharacterized relationship between the reaction rate constants governing tribromide formation and those governing bromine reduction.³⁷ For the

purpose of this work, this question is addressed by using the standard potential and diffusion coefficient for tribromide ions in place of bromine.^{35,38}

Inlet and Outlet Boundary Conditions

Electroneutrality dictates that zero flux boundary conditions are applied for the ionic potential at both the inlet and the outlet. At the outlet, zero diffusive flux boundary conditions are applied to both species. At the inlet, Dirichlet boundary conditions are imposed on both species. A constant initial acid concentration is applied to the entire inlet. The bromine is hydrodynamically focused to form a thin layer near the cathode by fixing an electrolyte to oxidant flow ratio of 10:1. For Poiseuille flow in a channel, this corresponds to an oxidant layer thickness of $y^* = 0.186h$ at the inlet.

Boundary Layer Analysis

The full model can be solved numerically with finite-element discretization (using COMSOL Multiphysics software, Burlington, MA), and results are given below. The numerical solution is valuable in that it allows for a deconstruction of the source of loss, and provides a tool to predict and understand the performance of experimental systems. However, it is computationally expensive to perform these simulations, and it would be desirable to derive simple formulae to predict the performance and behavior of any laminar flow system. This can be done by boundary-layer analysis for forced convection in the cases of plug flow and Poiseuille flow discussed earlier.²⁹ The simplest case to consider is a cell with fast reactions and highly conductive electrolyte operating at limiting current. In this case, reactant flows into the cell at $x = 0$ with a constant concentration and is quickly consumed at the electrode at $y = 0$, so the reactant concentration there is zero. Next, these assumptions are lifted, and the analytical

approximation is extended to under-limiting current and finite electrolyte conductivity, while maintaining good accuracy over a wide range of system parameters.

Plug Flow

This problem is a special case of advection-diffusion in potential flow past a slipping adsorbing boundary,^{39,40} which has been studied recently in the context of solidification from a flowing melt⁴¹ and particle aggregation or electrodeposition from flowing solutions.⁴² Here, potential flow can be justified if the flow channel is either filled with an uncharged porous medium or thin in the transverse (z) direction ($w \ll h, L$), like a single two-dimensional pore, or Hele-Shaw cell as shown in Figures 1b-c. In both cases, the flow is governed by Darcy's law, and the fluid pressure acts as a velocity potential. Although the assumption of plug flow may seem restrictive, the same solution can be conformally mapped to any geometry of potential flow in two dimensions, such as curved, bent, corrugated or rough channels.⁴¹⁻⁴³ This mathematical transformation, based on the conformal invariance of the Nernst-Planck equations with advection in potential flow,³⁹ preserves the scaling relationships derived below and underscores the generality of the boundary-layer theory.

To clarify scalings and simplify the analysis, the governing equation for reactant transport is made dimensionless by defining the Peclet number as $Pe = Uh/D_i$, along with the dimensionless position $(\tilde{x}, \tilde{y}) = (x/L, y/h)$, concentration $\tilde{c}_i = c_i/c_i^0$, and channel aspect ratio $\beta = L/h$. In the relevant limit of large Peclet numbers, advection dominates diffusion in the axial direction after a very short entrance region, $x \gg D_i/U$, or $\tilde{x} \gg (\beta Pe)^{-1}$. The advection-diffusion equation shown in Equation 4 then takes a very simple form,

$$\frac{\text{Pe}}{\beta} \frac{\partial \tilde{c}_i}{\partial \tilde{x}} = \frac{\partial \tilde{c}_i}{\partial \tilde{x}} = \frac{\partial^2 \tilde{c}_i}{\partial \tilde{y}^2}, \quad [12]$$

equivalent to the transient diffusion equation, where the distance traveled downstream in the plug flow is analogous to time for transverse diffusion between the electrodes. The appropriate dimensionless variable is the axial position, $\hat{x} = \frac{\tilde{x}\beta}{\text{Pe}} = x/x_e$, scaled to the entrance length, $x_e = Uh^2/D_i$, for forced convection.⁴³ The classical spreading solution of the diffusion equation yields a similarity solution for the reactant concentration,³⁹⁻⁴¹

$$\tilde{c}_i(\tilde{x}, \tilde{y}) = \text{erf}\left(\sqrt{\frac{\text{Pe}}{4\tilde{x}\beta}} \tilde{y}\right) = \text{erf}\left(\frac{\tilde{y}}{2\sqrt{\tilde{x}}}\right). \quad [13]$$

The solution describes a 99% depletion boundary layer of dimensionless thickness, $\delta = 3.64\sqrt{\hat{x}}$, having a parabolic shape, $\hat{x} \sim \tilde{y}^2$. Faraday's law can then be used to relate the reactant flux to the electrode to the local dimensionless current density $\tilde{j} = hj/nD_iFc_i^0$ along the length of the channel in terms of the number of moles of electrons transferred per mole of reactant n .

$$\tilde{j}_{lim}(\hat{x}) = \sqrt{\frac{1}{\pi\hat{x}}} \quad [14]$$

Poiseuille Flow

Next we consider viscous flow in a free electrolyte channel between the electrodes. If the electrode spacing is much thinner than the channel width, then fully developed, unidirectional flow can be assumed with a parabolic Poiseuille flow profile. At sufficiently high Peclet numbers, the depletion layer of reactant near the electrode is thin relative to the electrode spacing, and the quadratic term in the flow profile can be neglected to simplify the advection diffusion equation. The equation can be simplified further by neglecting axial diffusion, as was done in the plug flow case.

$$\frac{6\text{Pe}}{\beta} \tilde{y} \frac{\partial \tilde{c}_i}{\partial \tilde{x}} = 6\tilde{y} \frac{\partial \tilde{c}_i}{\partial \tilde{x}} = \frac{\partial^2 \tilde{c}_i}{\partial \tilde{y}^2} \quad [15]$$

This approximation for the advection-diffusion boundary layer in viscous shear flow at a no-slip surface was first proposed by L        ^{43,44} who obtained an exact solution widely used in theories of heat and mass transfer by forced convection⁴³ and electro dialysis.³⁴ The solution can be written in terms of the incomplete gamma function, $\Gamma(s, a)$.

$$\tilde{c}_i(\hat{x}, \hat{y}) = \Gamma(2\hat{y}^3/\hat{x}, 1/3)$$

$$\Gamma(s, a) = (\int_0^s e^{-t} t^{a-1} dt) / (\int_0^\infty e^{-t} t^{a-1} dt) \quad [16]$$

The 99% boundary layer thickness now scales as the cube-root of the axial position, $\tilde{\delta} = 1.11 \sqrt[3]{\hat{x}}$. Faraday's law can again be applied to this result to derive the local dimensionless limiting current distribution in terms of the complete Gamma function $\Gamma(a)$ using the same scaling as in the case of plug flow. A highly conductive electrolyte and fast reactions are assumed, therefore cell voltage will not change significantly until limiting current is reached, so the power of the system will be proportional to the limiting current.

$$\tilde{j}_{\text{lim}}(\hat{x}) = \sqrt[3]{\frac{18}{\hat{x}}} \frac{1}{\Gamma(1/3)} \quad [17]$$

The inverse cube root behavior of the limiting current along the length of the electrode is a general consequence of the boundary layer scaling noted above^{24,25,29} and also arises in the theory of electro dialysis.³⁴ The same analysis also generally relates the dimensionless flux in heat transfer (Nusselt number) or mass transfer (Sherwood number) to the Peclet number for forced convection in the entrance region of a pipe.⁴³ It stands in contrast to the inverse square root behavior of current density in the plug flow case, but in both cases, there is a maximum in current density near the inlet of the cell, followed by a gradual drop off along the length of the channel. Both of these results can also be integrated along the length of the channel to determine the average limiting current

density, as shown in Table 2. Although exact conformal invariance does not hold for viscous flow, the same scaling relationships also apply to advection-diffusion viscous flows in more complicated geometries.⁴³

Reactant Crossover

The absence of a physical barrier between the electrodes makes reactant crossover a primary concern in membraneless systems. The growth of the mixing layer in a laminar channel as reactants diffuse away from their respective electrodes into the separating electrolyte has been well described before, and can be directly applied here.²⁵ In the case of plug flow, there is no local strain rate, so the mixing region grows as $\delta_m = 3.64\sqrt{x}$ everywhere in the channel. This results in a maximum channel aspect ratio to ensure that the mixing region does not reach across the channel.

$$\beta_{\text{mixing}} \ll 0.0755 \text{ Pe} \quad [18]$$

In reality, this turns out not to be a major limitation on system design. In the example of the HBLFB, the channel would have to be almost a meter long before mixing became an issue.

The situation is more complicated for Poiseuille flow due to the variable strain rate across the channel. Near the center of the channel, the flow is nearly uniform, and the mixing region grows as $\delta_m \sim \sqrt{x}$, just like the plug flow case. However, as the mixing region nears the edges, the strain rate increases and the mixing region slows down to $\delta_m \sim \sqrt[3]{x}$. Numerical methods are required to solve for the intermediate regions between these two limits,^{24,25} but mixing region growth will be bounded by the plug flow case, and can again be ignored for most systems.

Reactant Utilization

In a real system, reactant utilization is also a significant concern, since low utilization hurts Coulombic efficiency and therefore overall energy efficiency. Utilization γ is defined as the ratio of reactant consumed at the electrode to total reactant flux into the channel, and can be expressed in terms of the initial location of the reactant electrolyte interface, \tilde{y}^* . For the case of plug flow,

$$\gamma = \frac{\beta \int_0^{\beta/\text{Pe}} \tilde{j}_{\text{lim}}(\hat{x}) d\hat{x}}{\int_0^{\tilde{y}^*} \tilde{u}(\tilde{y}) d\tilde{y}} = \frac{2}{\tilde{y}^*} \sqrt{\frac{\beta}{\pi \text{Pe}}}. \quad [19]$$

Comparing Equation 19 with the average current density in Table 2 shows that there is a tradeoff between utilization and limiting current density. Increasing the Peclet number or decreasing the aspect ratio will increase limiting current at the same rate that it decreases utilization, such that their product is a constant.

$$\gamma \cdot \bar{j}_{\text{lim}} = \frac{4}{\pi \tilde{y}^*} \quad [20]$$

As long as cell voltage is not heavily influenced by ohmic losses, this results in a balancing act between power and utilization. This inherent compromise must be considered in the design of any membraneless electrochemical cell. A similar analysis can be performed for Poiseuille flow, with the results for a thin reactant layer summarized in Table 2. As in the case of plug flow, an increase in current always results a decrease in utilization.

Regardless of the flow profile, decreasing \tilde{y}^* has the immediate effect of increasing utilization up to the point where the depletion boundary layer $\tilde{\delta}$ is thicker than the reactant layer \tilde{y}^* . This places an easily calculable upper limit on reactant utilization.

Under-limiting Current

In any type of flow, the boundary-layer theory for limiting current can be extended to more completely describe an electrochemical flow cell by allowing for under-limiting current and finite electrolyte conductivity, which to our knowledge has not been done before. For the case of the HBLFB, activation losses are assumed to be small, an assumption justified by Figure 3, but the technique described here could easily be modified to account for activation losses. As long as the current density in the channel remains one-dimensional, the system can be described by a local current-voltage relation expressed in terms of dimensionless potential $\tilde{\varphi} = F\varphi/RT$ and conductivity $\tilde{\sigma} = RT\sigma/nD_iF^2c_i^0$. For the reacting bromine in the HBLFB, $n = 2$.

$$\tilde{\varphi}_{cell} = \tilde{\varphi}_c^0 + \frac{1}{2} \ln(\tilde{c}_{Br_2}(\tilde{x})) - \tilde{j}(\tilde{x})/\tilde{\sigma} \quad [21]$$

If the conductivity becomes large, and the cell potential goes to a large negative value, Equation 21 returns the limiting current result from Equations 17 for Poiseuille flow. At finite cell potential and conductivity, the structure of the boundary layer is such that the local surface concentration changes slowly along the length of the channel relative to how it changes moving into the channel, so at every point along the electrode, the local current density can be expressed in terms of the local cathode surface concentration and the limiting current density summarized in Table 2.

$$\tilde{j}(\tilde{x}) = (1 - \tilde{c}_{Br_2}(\tilde{x}))\tilde{j}_{lim}(\tilde{x}) \quad [22]$$

Solving for $\tilde{c}_{Br_2}(\tilde{x})$ and substituting the result back into Equation 21 yields a current-voltage relation that can be implicitly solved for every point along the electrode.

$$\tilde{\varphi}_{cell} = \tilde{\varphi}_c^0 + \frac{1}{2} \ln\left(1 - \frac{\tilde{j}(\tilde{x})}{\tilde{j}_{lim}(\tilde{x})}\right) - \frac{\tilde{j}(\tilde{x})}{\tilde{\sigma}} \quad [23]$$

Equation 23 represents a general current-voltage relation for any laminar flow electrochemical cell with rapid ion removal at a surface. Since this relation is determined

by ion transport to an adsorbing surface, the same fundamental result, using the appropriate ionic species in Equations 21-22, could also be applied to electrodialysis in Poiseuille flow,⁴⁵ shock electrodialysis in plug flow⁴⁶ or any other membrane-based ion removal process in cross flow. The expression could be modified further to include anode concentration polarization or activation overpotential with no loss of generality. The impact of the flow profile on this expression is through the limiting current term, which can be specified to reflect the particular electrochemical cell being examined.

Results and Discussion

The HBLFB provides an example of a reversible membrane-less electrochemical cell with which to validate the theory presented in this work. In a recent article,⁴⁷ it was shown that numerical solutions of the full two-dimensional model provide an excellent fit to experimental current-voltage data for different flow rates and bromine concentrations for both charging and discharging of the cell. Our focus here is on testing the accuracy of the simple analytical expressions derived above by boundary layer analysis and discussing general engineering principles for membrane-less laminar flow electrochemical cells.

Under the conditions specified in Table 1, the numerical solution can be used to predict the concentration of bromine and hydrobromic acid in the channel, as shown in Figure 2. Hydrobromic acid flows into the cell at a concentration of 1 M, and enrichment layers develop at both electrodes along the length of the channels. The enrichment is greater at the cathode than the anode due to the asymmetry in diffusion coefficients between the bromide ions generated at the cathode and the protons generated at the anode. A bromine depletion layer develops along the cathode where bromine is consumed, while a mixing region develops at the top of the bromine layer as bromine diffuses into the

electrolyte. Eventually, these two regions begin to overlap, resulting in bulk depletion of the bromine. This is desirable from a reactant utilization perspective, since it means that a large fraction of the bromine is being consumed, but violates the analytical assumption that the bromine concentration is uniform far away from the cathode surface.

Another important result is that the current density drops rapidly along the length of the channel. Both the numerical and analytical models accurately predict this effect, as shown in Figure 3a. This behavior is in stark contrast to traditional membrane-based electrochemical systems where serpentine flow fields and other means are used to ensure that current density is approximately constant along the entire active area. This drop in current is due predominantly to the depletion of bromine at the cathode, as shown in Figure 3b. One implication of this behavior is that the diffusion of acid away from the electrodes eventually becomes faster than the generation of acid at the electrodes. The result is a maximum acid concentration near the channel inlet followed by a gradual reduction in acid concentration along the rest of the channel.

High electronic conductivity within the current collectors ensures that the anode and cathode potentials are constant along the length of the channel, but the large variations in reactant surface concentrations and current density mean that the source of losses varies strongly. Losses can be grouped into three categories: activation, concentration, and ohmic. Activation overpotential is the potential required to drive charge transfer at the electrodes, concentration polarization describes the variation in equilibrium potential from standard conditions due to the enrichment or depletion of reactants and products at the electrodes, and ohmic loss is simply the potential drop across the electrolyte.

These three sources of loss can be compared to each other along the length of the channel. These results are shown in Figure 3c, and confirm that activation overpotential is negligible as a result of the rapid reaction kinetics of both the bromine reduction reaction and the hydrogen oxidant reaction. This justifies ignoring activation losses in the analytical model. As expected, the strong spatial variation in species concentration and current density leads to variation in the source of loss along the length of the electrode, with ohmic losses dominating in the inlet region of the channel and concentration polarization rapidly building up towards the end of the channel. There is excellent agreement between the analytical and numerical predictions for ohmic and concentration losses along the length of the channel, which illustrates the predictive power of a lightweight analytical model to describe a numerically complex system.

The local current distribution predicted by the analytical and numerical models can also be integrated to calculate the average current density as a function of cell voltage. Because the analytical model treats only the dominant sources of loss- concentration polarization and ohmic losses- only four parameters are required to determine the analytical dimensionless current-voltage relation: aspect ratio, conductivity, Peclet number, and standard potential. For the purpose of this study, flow rate and reactant concentration are treated as model inputs. Figure 4a plots the predicted and observed current-voltage relation for the HBLFB during discharge as the Peclet number is varied from 5,000 to 15,000. The analytical model, which ignores activation overpotential completely, overestimates cell voltage at low current densities, but limiting current density is well described over a range of Peclet numbers.

The HBLFB employs reversible reactions at both electrodes, so both the analytical and numerical models can be easily applied to the cell during charging as well as discharging. Both the hydrogen oxidation reaction and the bromine reduction reaction are

known to be reversible, so both models can equally be applied to the case of charging. If an external current is applied the cell, the electrodes switch function so that hydrogen is evolved at the cathode, and bromine at the anode. Figure 4b plots the analytical, numerical, and experimental current-voltage relations for the HBLFB during charging as the electrolyte concentration is varied. Again, the analytical theory slightly overpredicts performance at intermediate voltages compared to the numerical simulation. The disparity is likely due to the enrichment of bromine along the anode resulting in an increase in cell voltage in the numerical simulation that is not considered in the analytical theory. Experimental data displays slightly higher limiting current than predicted, which is most likely due to the presence of side reactions at high voltage

Conclusion

This work develops general theoretical principles for the design and operation of membrane-less laminar flow electrochemical cells, and applies these techniques to the HBLFB as an example. Simple analytical results for different flow types, obtained by boundary layer analysis, provide a computationally inexpensive tool to rapidly examine the performance of laminar flow electrochemical cells in general by reducing the number of model parameters down to the minimum necessary to capture the dominant features of the system. Both the numerical and analytical models can be used to fit discharge and charging behavior and to identify the major sources of loss along the length of the channel. Predicted boundary layer profiles are also essential to guide the splitting of the anolyte and catholyte fluid streams leaving the electrode gap. Properly designed systems can reduce mixing and maximize reactant utilization or electrolyzed products, which is of particular importance for rechargeable electrochemical cells such as the HBLFB. These

models can be used to aid future design of membrane-less laminar flow electrochemical cells.

Similar models, augmented for bulk reactions, could also be applied to viscous flowable electrodes, as in semi-solid Li-ion flow batteries,^{48,49} flow supercapacitors,⁵⁰ and flow capacitive deionization.⁵¹ These unconventional cell architectures rely on membrane separators between the flowable electrodes, but in principle, any combination of the three major components of the cell could be designed for laminar cross flow. Understanding the effects of advection-diffusion boundary layer scaling on electrochemical behavior is critical for the efficient and safe operation of such systems.

On a fundamental level, the results of this work are in sharp contrast to the common practice of treating electrochemical cells as quasi one-dimensional, in which case the sources of loss within the system can easily be classified by fitting to polarization curves. When symmetry is broken by cross flow, the local current density and concentration determine the spatial distribution of losses, which strongly vary along the surface of the electrode. Under conditions examined in this work, no single source of loss is dominant along the entire channel. The precise distribution of losses will vary depending on operating conditions and specific cell design, but the general result that the source of loss is highly variable along the length of the electrode is applicable to a wide range of membrane-less laminar flow systems. The fact that electrochemical properties vary along the flow channel separating the electrodes, perpendicular to the current, also suggests that standard area-averaged figures of merit do not properly characterize the performance of flow batteries (regardless of whether or not there is a membrane). These metrics, such as the energy or power density per electrode area, should be replaced by other measures, such as coefficients in boundary layer approximations, which better capture the true, nonlinear scaling behavior of these systems.

References

1. R. Ferrigno, A. D. Stroock, T. D. Clark, M. Mayer, and G. M. Whitesides, *J. Am. Chem. Soc.*, **124**, 12930–12931 (2002).
2. E. R. Choban, L. J. Markoski, A. Wieckowski, and P. J. A. Kenis, *J. Power Sources*, **128**, 54–60 (2004).
3. E. Kjeang, R. Michel, D. A. Harrington, N. Djilali, and D. Sinton, *J. Am. Chem. Soc.*, **130**, 4000–4006 (2008).
4. S. A. Mousavi Shaegh, N.-T. Nguyen, and S. H. Chan, *Int. J. Hydrogen Energ.*, **36**, 5675–5694 (2011).
5. E. Kjeang, N. Djilali, and D. Sinton, in *Advances in microfluidic fuel cells*, p. 99–139, Elsevier (2009).
6. Tiax, LLC, *Cost Analysis of Fuel Cell Systems for Transportation*, p. 46, (2004), p. 1–46.
7. F. R. Brushett et al., *J. Am. Chem. Soc.*, **132**, 12185–12187 (2010).
8. F. R. Brushett, W.-P. Zhou, R. S. Jayashree, and P. J. A. Kenis, *J. Electrochem. Soc.*, **156**, B565 (2009).
9. M. S. Naughton, F. R. Brushett, and P. J. A. Kenis, *J. Power Sources*, **196**, 1762–1768 (2011).
10. D. A. Finkelstein, J. D. Kirtland, N. D. Mota, A. D. Stroock, and H. D. Abruña, *J. Phys. Chem. C*, **115**, 6073–6084 (2011).

11. N. Da Mota et al., *J. Am. Chem. Soc.*, **134**, 6076–6079 (2012).
12. E. Kjeang et al., *Electrochim. Acta*, **52**, 4942–4946 (2007).
13. A. S. Hollinger et al., *J. Power Sources*, **195**, 3523–3528 (2010).
14. R. S. Jayashree et al., *J. Am. Chem. Soc.*, **127**, 16758–16759 (2005).
15. A. D. Stroock et al., *Science*, **295**, 647–651 (2002).
16. P. Tabeling, M. Chabert, A. Dodge, C. Jullien, and F. Okkels, *Philos Trans A Math Phys Eng Sci*, **362**, 987–1000 (2004).
17. S. A. Mousavi Shaegh, N.-T. Nguyen, S. H. Chan, and W. Zhou, *Int. J. Hydrogen Energ.*, **37**, 3466–3476 (2012).
18. J. W. Lee, M.-A. Goulet, and E. Kjeang, *Lab Chip*, **13**, 2504–2507 (2013).
19. A. Bazylak, D. Sinton, and N. Djilali, *J. Power Sources*, **143**, 57–66 (2005).
20. R. S. Jayashree et al., *J. Power Sources*, **195**, 3569–3578 (2010).
21. J. Xuan, M. K. H. Leung, D. Y. C. Leung, M. Ni, and H. Wang, *Int. J. Hydrogen Energ.*, **36**, 11075–11084 (2011).
22. I. B. Sprague, D. Byun, and P. Dutta, *Electrochim. Acta*, **55**, 8579–8589 (2010).
23. I. B. Sprague and P. Dutta, *Electrochim. Acta*, **56**, 4518–4525 (2011).
24. R. F. Ismagilov, A. D. Stroock, P. J. A. Kenis, G. Whitesides, and H. A. Stone, *Appl. Phys. Lett.*, **76**, 2376 (2000).
25. J. Jiménez, *J. Fluid Mech.*, **535**, 245–254 (2005).

26. W. A. Braff and C. R. Buie, *ECS Trans.*, **33**, 179–190 (2011).
27. I. B. Sprague and P. Dutta, *SIAM J. Appl. Math.*, **72**, 1149–1168 (2012).
28. J. Newman and K. E. Thomas-Alyea, *Electrochemical Systems*, 3rd ed. p. 1, John Wiley, (2004).
29. M. Z. Bazant, *10.626 Electrochemical Energy Systems*, License: Creative Commons BY-NC-SA. Massachusetts Institute of Technology Open Courseware, (2011)
<http://ocw.mit.edu>.
30. P. M. Biesheuvel, M. van Soestbergen, and M. Z. Bazant, *Electrochim. Acta*, **54**, 4857–4871 (2009).
31. M. Z. Bazant, *Acc. Chem. Res.*, **46**, 1144–1160 (2013).
32. I. B. Sprague and P. Dutta, *Electrochim. Acta*, **91**, 20–29 (2013).
33. W. Cooper and R. Parsons, *Trans. Faraday Soc.*, **66**, 1698–1712 (1970).
34. R. F. Probstein, *Physicochemical Hydrodynamics*, p. 1, Wiley-Interscience, (1989).
35. D. R. Lide, *Handbook of Chemistry and Physics*, p. 1, CRC Press, (2012).
36. R. W. Ramette and D. A. Palmer, *J. Solution Chem.*, **15**, 387–395 (1986).
37. P. K. Adanuvor, R. E. White, and S. E. Lorimer, *J. Electrochem. Soc.*, **134**, 1450–1454 (1987).
38. A. J. Bard, R. Parsons, and J. Jordan, *Standard Potentials in Aqueous Solution*, p. 1, Marcel Dekker, Inc., New York, NY, (1985).

39. M. Z. Bazant, *Proceedings of the Royal Society A: Mathematical, Physical and Engineering Sciences*, **460**, 1433–1452 (2004).
40. J. Choi, D. Margetis, T. M. Squires, and M. Z. Bazant, *J. Fluid Mech.*, **536**, 155–184 (2005).
41. L. M. Cummings, Y. E. Hohlov, S. D. Howison, and K. Kornev, *J. Fluid Mech.*, **378**, 1–18 (1999).
42. M. Z. Bazant, J. Choi, and B. Davidovitch, *Phys. Rev. Lett.*, **91** (2003).
43. W. M. Deen, in, p. 664, Oxford University Press (2012).
44. A. L  v  que, *Annales des Mines*, **13**, 284 (1928).
45. A. A. Sonin and R. F. Probstein, *Desalination*, **5**, 293–329 (1968).
46. D. S. Deng et al., *submitted* (2013).
47. W. A. Braff, M. Z. Bazant, and C. R. Buie, *Nat. Commun.* (2013).
48. M. Duduta et al., *Adv. Energy Mater.*, **1**, 511–516 (2011).
49. V. E. Brunini, Y.-M. Chiang, and W. C. Carter, *Electrochim. Acta*, **69**, 301–307 (2012).
50. V. Presser et al., *Adv. Energy Mater.*, **2**, 895–902 (2012).
51. S.-I. Jeon et al., *Energy Environ. Sci.*, **6**, 1471–1475 (2013).

Table 1. Model parameters for the Hydrogen Bromine Laminar Flow Battery.

Parameter	Symbol	Value
Ideal gas constant	R	8.314 J/mol K
Temperature	T	298 K
Faraday's constant	F	96485 C/mol
Channel height	h	800 μm
Channel length	L	1.30 cm
Mean flow velocity	U	1.44 cm/s
Br ₂ diffusion coefficient	D_{Br_2}	$1.15 \times 10^{-5} \text{ cm}^2/\text{s}$
Br ⁻ diffusion coefficient	D_{Br^-}	$2.08 \times 10^{-5} \text{ cm}^2/\text{s}$
H ⁺ diffusion coefficient	D_{H^+}	$9.31 \times 10^{-5} \text{ cm}^2/\text{s}$
Br ₂ exchange current density	K_c^0	0.5 A/cm ²
HBr exchange current density	K_a^0	0.5 A/cm ²
Br ₂ inlet concentration	$c_{\text{Br}_2}^0$	1.0 M
HBr inlet concentration	c_{HBr}^0	1.0 M
Cell potential	φ_{cell}	0.900 V

Table 2. Comparison of limiting current behavior for plug flow and Poiseuille flow profiles predicted by boundary-layer analysis expressed in terms of Peclet number Pe , aspect ratio β , dimensionless reactant layer thickness \tilde{y}^* , and dimensionless channel position (\hat{x}, \tilde{y}) .

Variable	Plug Flow	Poiseuille Flow
Flow profile $\tilde{u}(\tilde{y})$	Pe	$6Pe(\tilde{y} - \tilde{y}^2)$
Local current density $\tilde{j}_{lim}(\hat{x})$	$\sqrt{1/\pi\hat{x}}$	$\sqrt[3]{18/\hat{x}}/\Gamma(1/3)$
Average current density \bar{j}_{lim}	$2\sqrt{Pe/(\pi\beta)}$	$3\sqrt[3]{9Pe/(4\beta)}/\Gamma(1/3)$
99% depletion layer thickness δ	$3.64\sqrt{\hat{x}}$	$1.11\sqrt[3]{\hat{x}}$
Reactant utilization γ	$(2/\tilde{y}^*)\sqrt{\beta/(\pi Pe)}$	$(3\beta/(2Pe))^{2/3}/(\tilde{y}^{*2}\Gamma(1/3))$

Figure 1.

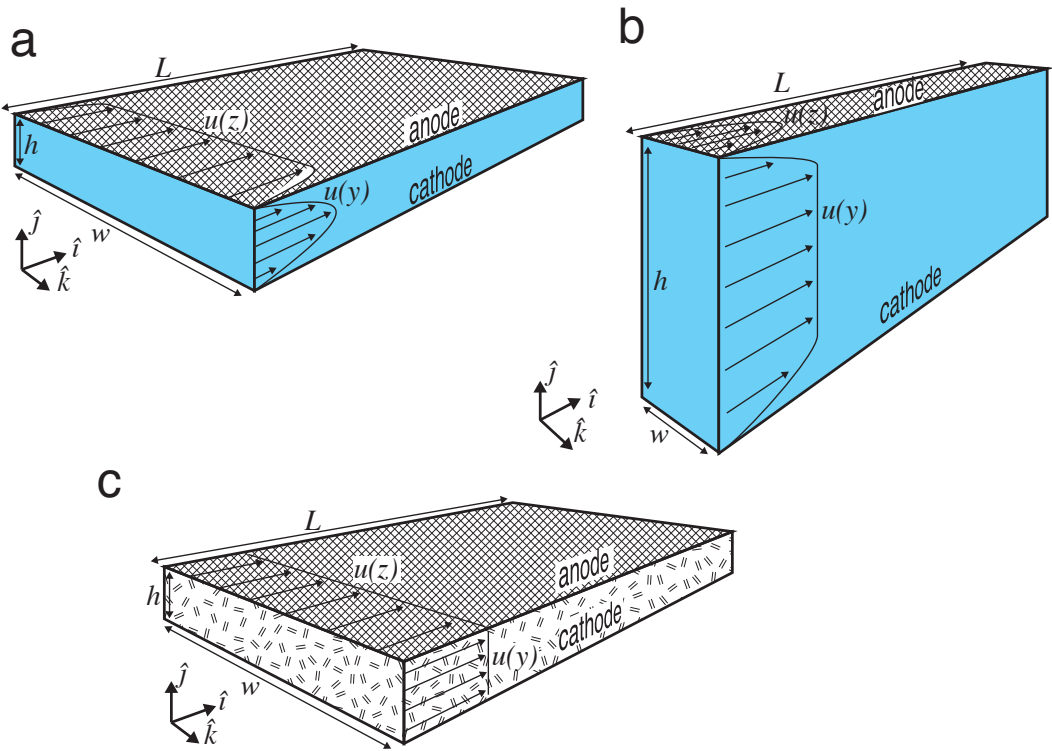


Figure 2.

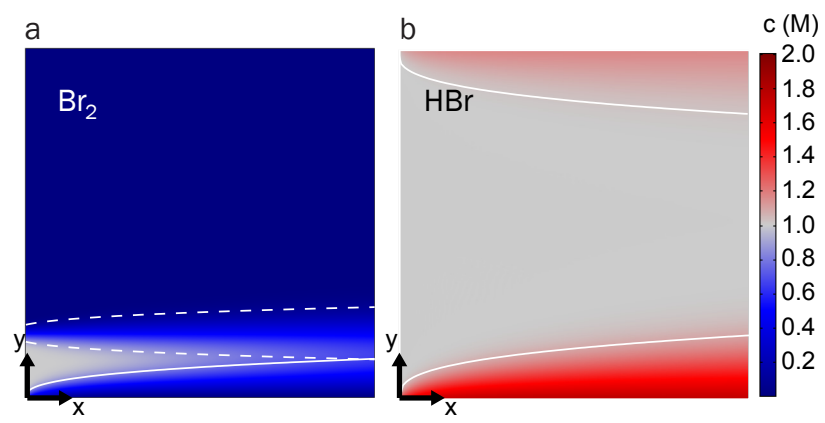


Figure 3.

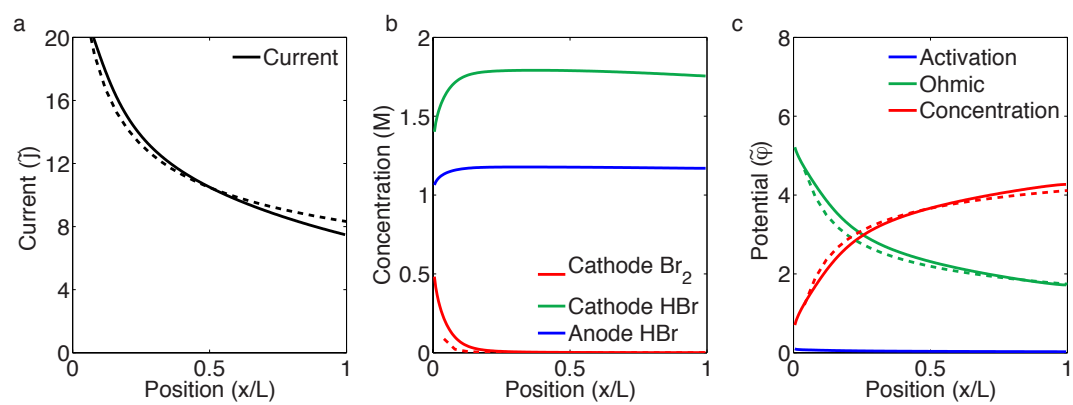


Figure 4.

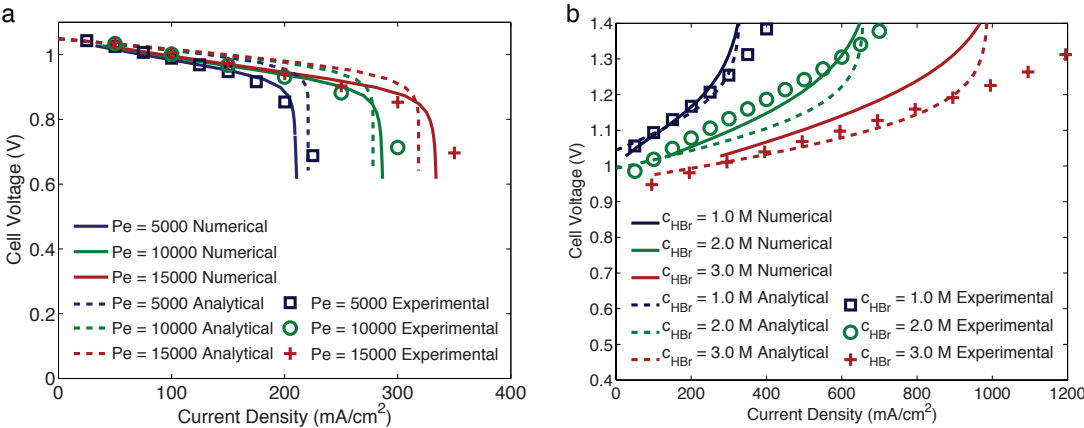


FIGURE CAPTIONS

Figure 1. Domain for the membrane-less electrochemical cell model. For wide, short channels (a), a parabolic flow profile can be assumed. For tall, narrow channels (b), a depth-averaged plug flow profile can be assumed. If the channel contains a porous medium (c), the flow profile will be similar to (b).

Figure 2. Concentration distribution of (a) bromine and (b) hydrobromic acid inside the channel under the conditions specified by Table 1. Depletion and enrichment layers derived from the boundary layer analysis are superimposed as solid white lines. Estimated reactant mixing zones that assume a linear velocity profile near the electrode wall are superimposed as dashed white lines.

Figure 3. (a) Local current density, (b) concentrations of bromine and hydrobromic acid, and (c) activation, ohmic, and concentration polarization losses along the length of the channel of the HBLFB for conditions listed in Table 1. Numerical results are shown as solid lines, with the analytical model overlaid as dashed lines. The dimensionless current density in the channel drops rapidly from a maximum at the inlet due to the sharply dropping bromine concentration at the cathode. Activation losses in the analytical model are negligible, and concentration polarization rises along the length of the channel to ensure constant electrode potential.

Figure 4. Numerical, (solid lines) analytical, (dashed lines) and experimental (symbols) current-voltage relations for the HBLFB at the conditions in Table 1 during (a) discharge as the Peclet number is varied from 5,000 to 15,000 and (b) charging as acid concentration is varied from 1 to 3 M.